JACS Au
AN OPEN ACCESS JOURNAL OF THE AMERICAN CHEMICAL SOCIETY

pubs.acs.org/jacsau
Article

Design Principle of Molybdenum-Based Metal Nitrides for Lattice Nitrogen-Mediated Ammonia Production

Shuairen Qian, Tianying Dai, Kai Feng, Zhengwen Li, Xiaohang Sun, Yuxin Chen, Kaiqi Nie, Binhang Yan, and Yi Cheng*

Cite This: *JACS Au* 2024, 4, 1975−1985
Read Online

ACCESS | Metrics & More | Article Recommendations | Supporting Information

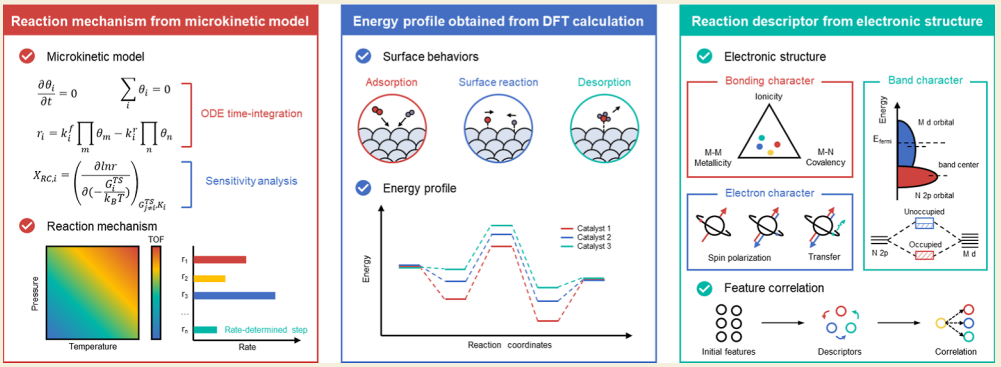

ABSTRACT: Chemical looping ammonia synthesis (CLAS) is a promising technology for reducing the high energy consumption of the conventional ammonia synthesis process. However, the comprehensive understanding of reaction mechanisms and rational design of novel nitrogen carriers has not been achieved due to the high complexity of catalyst structures and the unrevealed relationship between electronic structure and intrinsic activity. Herein, we propose a multistage strategy to establish the connection between catalyst intrinsic activity and microscopic electronic structure fingerprints using density functional theory computational energetics as bridges and apply it to the rational design of metal nitride catalysts for lattice nitrogen-mediated ammonia production. Molybdenum-based nitride catalysts with well-defined structures are employed as prototypes to elucidate the decoupled effects of electronic and geometrical features. The electron-transfer and spin polarization characteristics of the magnetic metals are constructed as descriptors to disclose the atomic-scale causes of intrinsic activity. Based on this design strategy, it is demonstrated that Ni_3Mo_3N catalysts possess the highest lattice nitrogen-mediated ammonia synthesis activity. This work reveals the structure−activity relationship of metal nitrides for CLAS and provides a multistage perspective on catalyst rational design.

KEYWORDS: *chemical looping ammonia synthesis, metal nitride catalysts, multistage design strategy, density functional theory, electronic structure, microkinetic modeling*

1. INTRODUCTION

Ammonia (NH_3) plays a crucial role both in agriculture as a fertilizer and in the chemical industry as a raw material.[1,2] Nowadays, ammonia is also an ideal candidate as a carbon-free energy carrier for the sustainable development of human society.[3] The conventional Haber−Bosch process catalyzed by fused iron catalysts is operated under high temperatures and pressures due to both thermodynamic and kinetic constraints, resulting in substantial energy consumption and global carbon emissions.[4−6] Although achieving ammonia production under atmospheric pressure is the cornerstone to reducing energy consumption, the strong coupling of thermodynamics and kinetics hinders the reduction of operation pressures while maintaining current production capacity. Therefore, the conventional ammonia process struggles to align with the imperatives of sustainable development. The chemical looping process emerges as a promising technology for atmospheric pressure ammonia synthesis as it enables the ammonia synthesis to be divided into several independent steps, which leads to the breaking of thermodynamic limits and individual process intensification for each process.[7−10] It is reported that the chemical looping ammonia synthesis (CLAS) process can achieve ammonia production through the interconversions between redox pairs of the nitrogen carriers.[11] Typically, metal nitrides are classical nitrogen carrier materials for both CLAS

Received: March 2, 2024
Revised: April 30, 2024
Accepted: May 1, 2024
Published: May 10, 2024

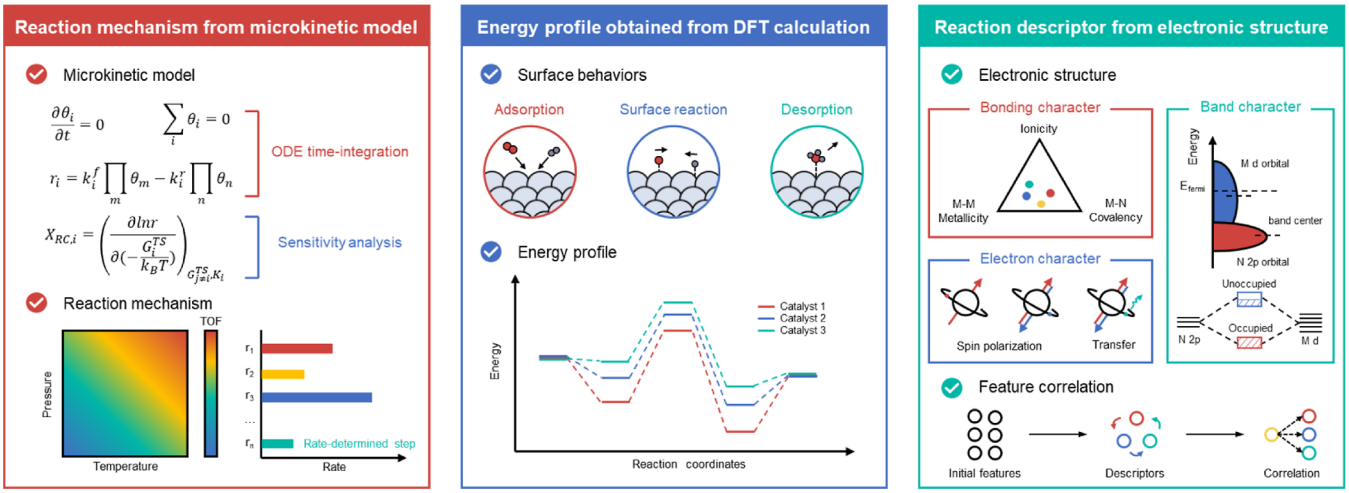

Figure 1. Multistage strategy to design metal nitrides for lattice nitrogen-mediated ammonia production. Schematic diagram of establishing the connection between catalyst intrinsic activity and microscopic electronic structure fingerprints using DFT computational energetics as bridges and rational design for novel efficient catalysts.

processes[7,12−15] and conventional ammonia synthesis processes via the lattice nitrogen-involved MvK mechanism.[16−20] In addition, metal nitrides also have great potential in the field of electrochemical N_2 to ammonia due to their unique structures.[21−27] Unfortunately, the introduction of N induces significant changes in the electronic properties and geometric features of nitrides compared to pure metals, and the complexity of chemical composition might have an immeasurable impact on the reaction performance.[28−31] These characteristics lead to the development of novel nitrogen carriers remaining in the inefficient trial-and-error approach. Recently, rational design of catalysts employing energetics descriptors based on density functional theory (DFT) calculations and structure descriptors based on the combinations of physical quantities has attracted much attention.[32−36] Nevertheless, these microscopic-level quantitative features are commonly correlated with the energetics based on DFT calculations rather than the intrinsic activity of catalysts, and the substantial gap between reaction rates and DFT energetics might yield completely conflicting conclusions.[37] The development of multistage models for heterogeneous catalysis bridges the gap between atomic-level electronic structure and intrinsic activity and provides the insights into reaction mechanisms, rate-determining steps (RDSs), and other pivotal reaction information.[38−40] This paradigm shift creates a robust foundation for the rational design of heterogeneous catalysts.

In this study, we propose a multistage design strategy to establish the connection between catalyst intrinsic activity and microscopic electronic structure fingerprints using DFT computational energetics as bridges (Figure 1). Molybdenum-based metal nitride catalysts (i.e., Co_3Mo_3N, Fe_3Mo_3N, Ni_3Mo_3N, and Mo_2N), a class of nitride materials with well-defined structures modified by magnetic metals, are employed as model catalysts for lattice nitrogen-mediated ammonia production to decouple the effects of electronic properties and geometrical features.[41−45] A combination of DFT calculations, electronic structure analysis, and microkinetic modeling (MKM) has been performed to identify the reaction mechanisms and feature descriptors by correlating the intrinsic activity with the electronic structure. The electron transfer between Mo and magnetic metals and the spin polarization characteristics of the magnetic metals are regarded as descriptors to uncover the atomic-scale causes of intrinsic activity. Thereafter, model nitride catalysts are synthesized and evaluated for CLAS performance. A series of *in situ* characterizations and activation experiments confirm the results of the applicability of this design strategy, realizing the paradigm shift from trial-and-error approach to rational design for metal nitride catalysts on a broader scale.

2. RESULTS AND DISCUSSION

2.1. Reaction Mechanisms for Lattice Nitrogen-Mediated Ammonia Synthesis

Molybdenum-based bimetallic nitrides modulated by magnetic transition metals (Fe, Co, and Ni) are a class of materials with well-defined structures (Figure 2a). The magnetic metals possess similar atomic radii and assembly, while exhibiting metallic states without covalent interactions with lattice N, thereby modulating the electronic structure of the nitrides with little change in geometrical characteristics.[34,46] Therefore, this is a well-characterized model to decouple the electronic regulation and geometric modulation of the active sites. We have established the lattice nitrogen-mediated ammonia synthesis reaction network over these nitrides and performed systematic DFT calculations, and the energetics are summarized in Figure 2b and Table S1. Compared to the NH_x hydrogenation and NH_3 desorption processes, N_2 dissociation and N replenishment processes possess lower energy barriers, indicating that N_2 dissociation might not be the rate-determining step, which is different from conventional industrial ammonia catalysts.[47] For Mo_2N, the extremely low energy barrier for N_2 dissociation (0.37 eV) is related to the nitrophilicity of Mo.[48,49] The reaction potential energy surface similarly demonstrates a stronger interaction between Mo and N (Figure 2c). The binding between Mo_2N and the intermediate species is too thermodynamically stable, contributing to the poor chemical looping of ammonia synthesis activity. In contrast, the modulation of magnetic metals weakens the Mo−N interaction and breaks the thermodynamic traps, which leads to a more efficient ammonia synthesis performance, as evidenced by a decrease in the energy barriers for N replenishment and NH_x species hydrogenation processes. However, we are currently unable to quantitatively measure the reaction rate and determine the rate-determined

https://doi.org/10.1021/jacsau.4c00194
JACS Au 2024, 4, 1975−1985

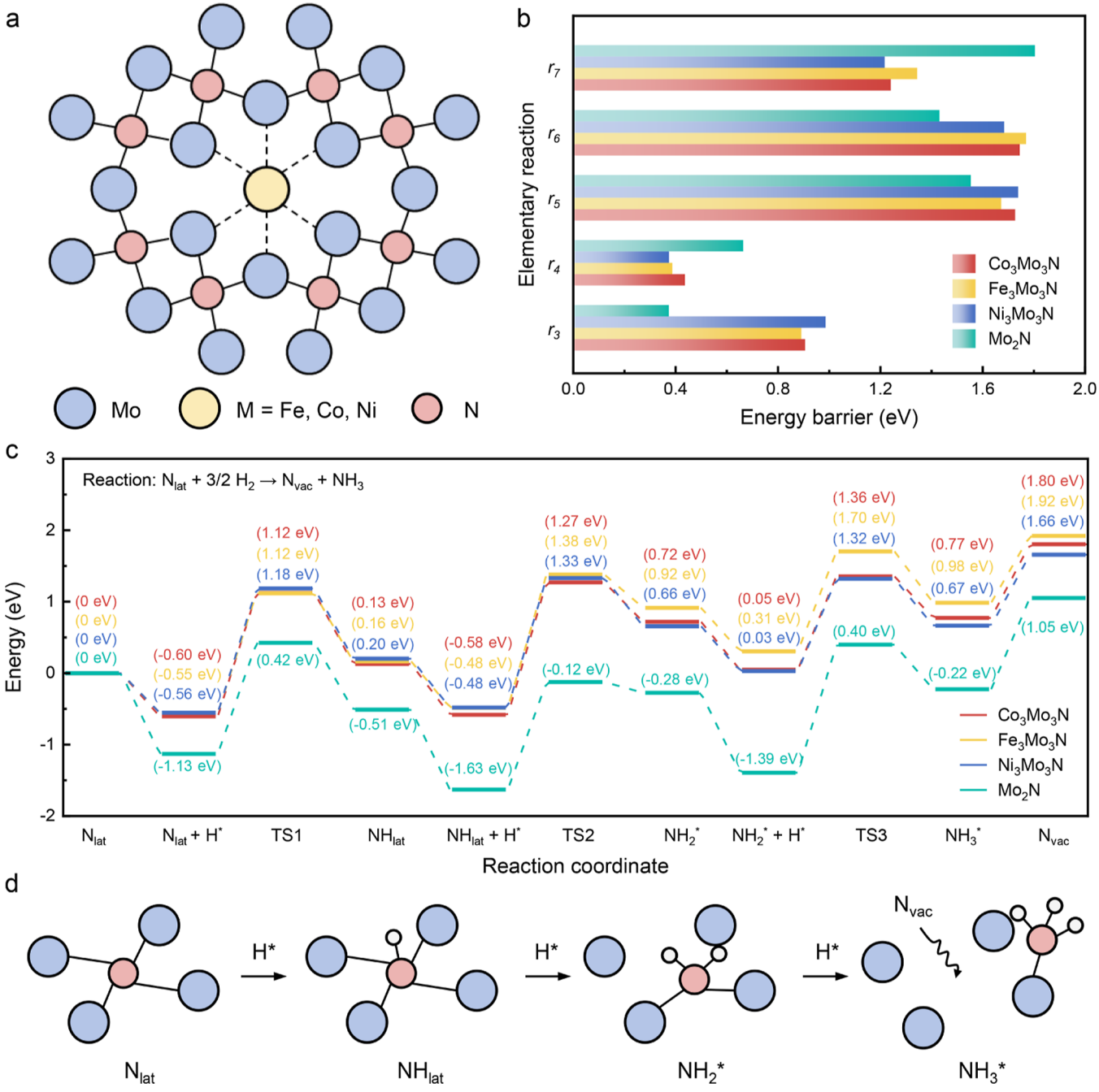

Figure 2. Reaction mechanisms and energetics of molybdenum-based metal nitrides. (a) Schematic diagram of molybdenum-based bimetallic nitrides. (b) Elementary reaction energetics of lattice nitrogen-mediated ammonia synthesis. (c) Reaction potential energy surface for ammonia synthesis. (d) Schematic representation of lattice nitrogen coordination structure for the hydrogenation process.

step since the reaction rate (or turnover frequency, TOF) is usually related to the energy span rather than the highest energy barrier of the elementary steps.[50,51] Therefore, we need to employ an approach beyond the molecular level to establish a structure−activity relationship between active sites and the reaction performance.

2.2. Microkinetic Insights into Lattice Nitrogen Activity

In an attempt to validate the predicted improvement in the catalytic activity through the modulation of magnetic transition metals and establish the structure−activity relationship, we have further conducted a mean-field MKM on the basis of the above reaction mechanisms. As shown in Figure 3, compared to the Mo_2N catalyst, Co_3Mo_3N, Fe_3Mo_3N, and Ni_3Mo_3N catalysts exhibit significant improvement of more than 1 order of magnitude in terms of reactivity, especially in the low-temperature region (the kinetic-controlled region). We take out the reaction performance curves at 1 bar to illustrate the differences between the magnetic metal modifications (Figure 3e). For the molybdenum-based nitride catalysts, the reactivity follows the order Ni_3Mo_3N > Co_3Mo_3N > Fe_3Mo_3N > Mo_2N. In low-temperature regions (less than 700 K), Mo_2N has extremely low reactivity for ammonia synthesis. As the temperature increases, the reaction activity of Mo_2N increases significantly, even exceeding that of the Fe_3Mo_3N catalysts. The isothermal curves of reactivity show similar trends, and the reaction

https://doi.org/10.1021/jacsau.4c00194
JACS Au 2024, 4, 1975−1985

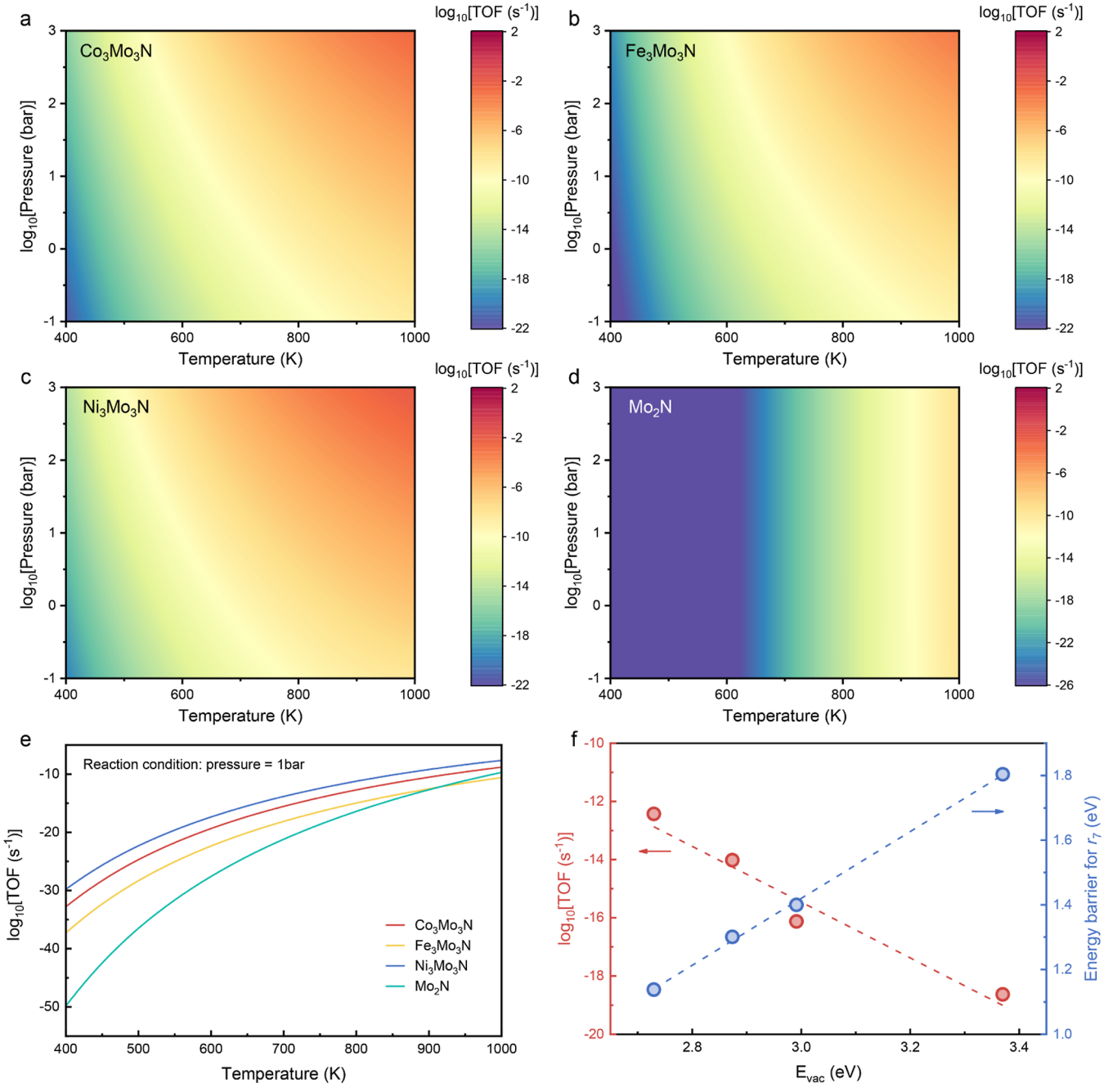

Figure 3. Reaction performance on the microkinetic scale. Lattice nitrogen-mediated ammonia synthesis rate (TOF) as a function of temperature and pressure at N_2/H_2 = 1:3 on (a) Co_3Mo_3N, (b) Fe_3Mo_3N, (c) Ni_3Mo_3N, and (d) Mo_2N catalysts. (e) Lattice nitrogen-mediated ammonia synthesis rate (TOF) as a function of temperature at 1 bar and N_2/H_2 = 1:3. (f) Relationship between N vacancy formation energy and ammonia synthesis rate (red) and energy barriers of the NH_2 species hydrogenation process (blue).

performance of the Mo_2N catalyst is insensitive to the reaction pressure (Figure S6). We also estimate the overall activation energies of different catalysts by the microkinetic model at 1 bar (Figure S7). The activation energy of Mo_2N is higher than those of other modified catalysts, which manifests the temperature sensitivity of the reaction activity. Therefore, the modulation of magnetic metals is a promising strategy to achieve efficient lattice nitrogen-mediated ammonia synthesis process. These results are in some contradiction with the experimental results in the previous literature studies, which will be discussed later.[52,53] In addition, we have also performed the degree of rate control (DRC) analysis, which is a powerful tool for identifying the rate-determining steps [or rate-determining transition states (TSs) and intermediates].[54−56] The results show that the lattice N hydrogenation behavior on these nitride surfaces follows a single rate-determining step mechanism controlled by NH_2^* hydrogenation (Figure S8). Furthermore, we correlate the ammonia synthesis rate with the DFT-based energy through N vacancy formation energy (E_{vac}), a universal factor of lattice N activity.[7,57] Specifically, TOF and the energy barrier of the rate-determining step (i.e., r_7) exhibit almost linear dependences on N vacancy formation energy as shown in Figure 3f. Hence, the N vacancy formation energy is a valid descriptor to reveal the

https://doi.org/10.1021/jacsau.4c00194
JACS Au 2024, 4, 1975−1985

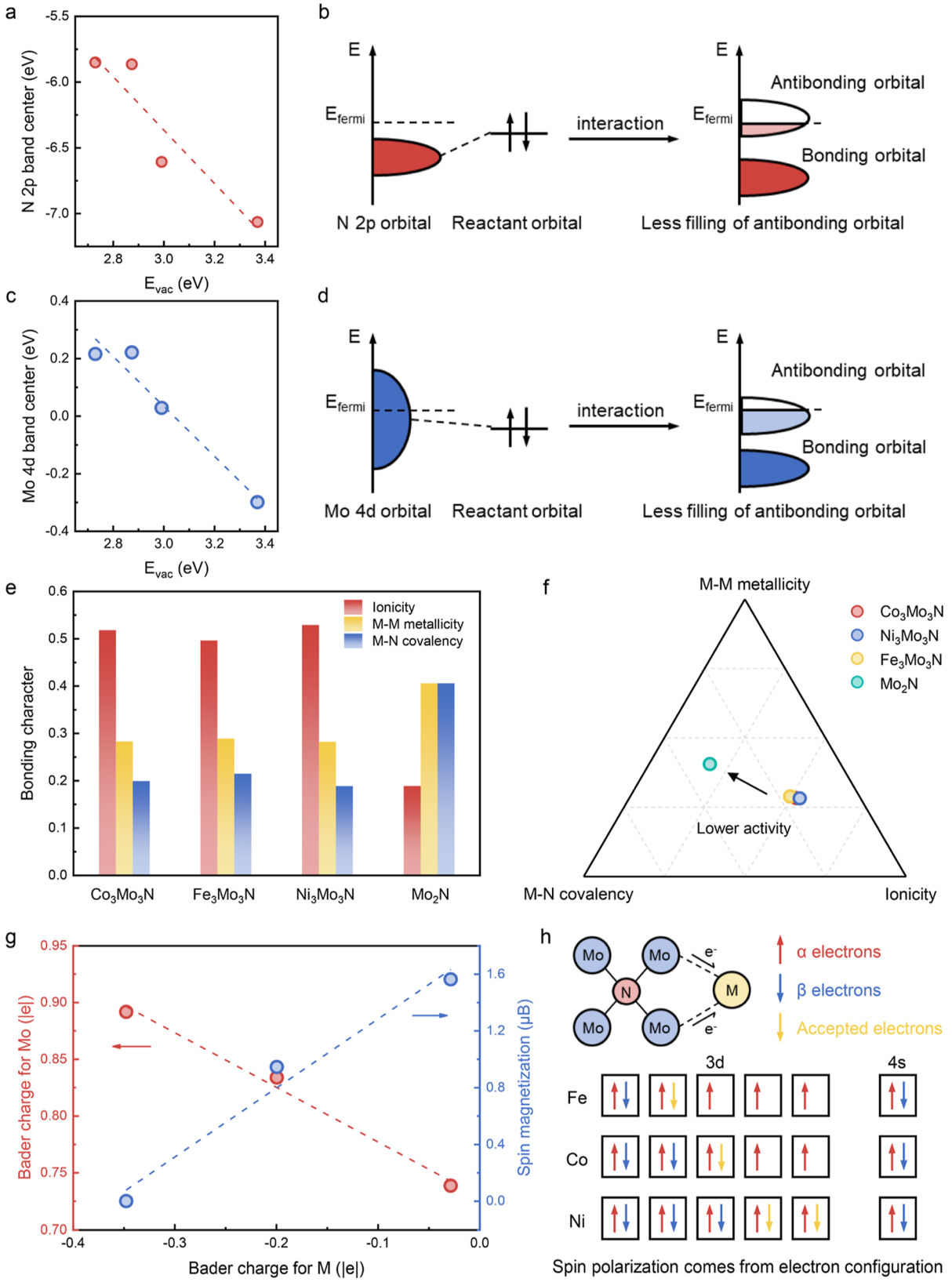

Figure 4. Electronic structure characteristics and potential descriptors for transition metal nitrides. Trends in (a) nitrogen 2p band center and (c) molybdenum 4d band center as a function of N vacancy formation energy. Orbital interaction analysis for (b) N 2p orbital and (d) Mo 4d orbital. (e) Bonding characteristics (M−M metallicity, M−N covalency, and ionicity) of metal nitrides. (f) Bonding characteristics plotted on the van Arkel−Ketelaar diagram. (g) Trends in Bader charge transfer of Mo (red) and spin magnetization of magnetic metals (blue) as a function of Bader charge transfer of magnetic metals. (h) Schematic diagram of the relationship between charge transfer and spin magnetization.

https://doi.org/10.1021/jacsau.4c00194
JACS Au 2024, 4, 1975−1985

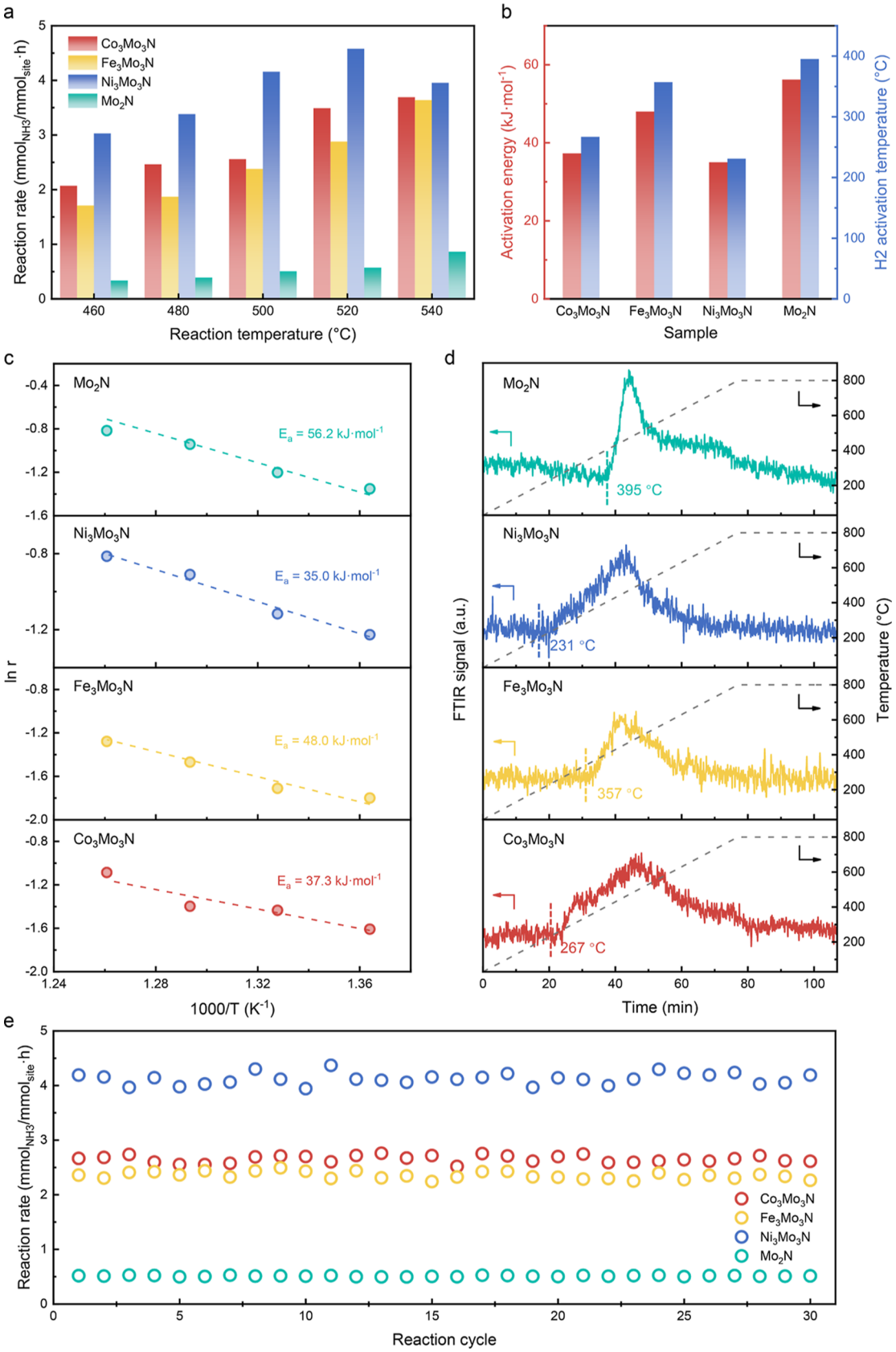

Figure 5. Nitride-mediated CLAS performance. (a) Reaction rate as a function of temperature. (b) Lattice N activation capacity, reflected as reaction activation energy (red) and H_2-TPR activation temperature (blue). (c) Analysis of the apparent activation energy (E_a) for ammonia synthesis. (d) H_2-TPR curves for metal nitride catalysts. (e) Stability test for CLAS at 500 °C. Reaction conditions: atmospheric pressure, 100 mg of catalyst, total flow rate = 40 mL/min, and Ar/H_2 = 1:3.

https://doi.org/10.1021/jacsau.4c00194
JACS Au 2024, 4, 1975−1985

lattice nitrogen-mediated ammonia synthesis rate for metal nitrides.

2.3. Electronic Structure Descriptors of Transition Metal Nitrides

Electronic structure analysis is a necessary tool to excavate the origins of the reaction activity and provide insights into the nature of the active sites. Typically, band characteristics,[58,59] bonding characteristics,[29,57,60] and charge-transfer/spin polarization characteristics[61−63] are common electronic structure analysis methods for elucidating the intrinsic properties of active sites. The lattice N hydrogenation process and the adsorption configurations of intermediate species are just shown in Figure 2d. Interestingly, the limited coordination ability of lattice N leads to the fact that the lattice N is pulled out of the solid surface, and the hydrogenation process becomes a surface reaction when the NH_2^* species is formed. Therefore, both the electronic structures of the clean surface and defective surface have an impact on lattice nitrogen-mediated ammonia synthesis activity. The projected density of states (PDOS) of the clean surface and defective surface and band center, a classical descriptor for measuring interactions in catalytic reactions, were carried out (Figure S9).[64,65] The N 2p band center of the clean surface exhibits a linear dependence on the N vacancy formation energy, which is attributed to a stronger hydrogenation interaction and lower antibonding orbital filling (Figure 4a,b). Similar conclusions can be drawn for the defective surface. The rate-determining step of NH_2^* hydrogenation implies that stabilizing the TS species (NH_2−H) facilitates the acceleration of overall reaction rate, which requires a lower Mo 4d band center (Figure 4c,d).[56] These can be taken as typical features, essentially reflecting the bonding ability between the surface and active lattice species (or adsorbed species). To further support this conclusion, the bonding characteristics based on the DFT-computed electron density and wave function are calculated (Figure 4e). Modulation of magnetic metals enhances the ionicity and weakens the covalency and metallicity for molybdenum-based metal nitrides (Figure 4f), which is consistent with the electron localization function diagrams (Figure S10). The decrease in covalency means that the catalyst is not as capable of constraining the lattice N and thus possesses an excellent reaction performance. Furthermore, it is found that magnetic metals exhibit different asymmetric behaviors of α and β orbitals in PDOS (Figure S9), thus the spin magnetic moment as well as the charge transfer which might be the unique fingerprint for such bimetallic nitrides. We first analyze the electronic effect of coordinated Mo on the lattice N activity. The oxidation state of Mo favors the activation of lattice N, which has been reported in our previous work.[45] Therefore, the charge transfer of Mo exhibits a good linear relationship with the N vacancy formation energy (Figure S17). Interestingly, the magnetization of magnetic metals also exhibits a linear dependence on the N vacancy formation energy (Figure S17). It is no coincidence that the relationship between charge transfer and magnetization of magnetic metals can be established through the electronegativity. Miedema has proposed a correlation between the charge transfer and electronegativity for transition metals.[66] As shown in Figure 4h, the electronegativity of modified metals (Fe, Co, and Ni) is slightly larger than that of Mo, exhibiting the electron transfer from Mo to modified metals. As the electronegativity difference increases, the transferred electrons populate on modified metals and compensate for unpaired electrons, leading to a decrease in the spin magnetic moment. The linear correlation between the charge transfer and magnetization well justifies this argument (Figure 4g). The *quasi in situ* X-ray photoelectron spectroscopy (XPS) experiments are also performed to prove this conclusion, and the value of the Mo 3d energy level shift to higher binding energies measures the degree of electron transfer (Figure S18). It is worth mentioning that the small electronegativity difference (∼0.1) can also explain the origins of modified metals presenting in metallic states. We have also performed a series of DFT calculations and microkinetic models without spin polarization to construct the lack of electron transfer (details in the Supporting Information). With the removal of the spin effect, the energy barriers of elementary reactions and overall rates decrease drastically. The rate-determining step is also shifted due to the change in the ability to stabilize the surface species (Figure S23). In summary, the ionic characteristics of the solid catalysts and the charge transfer of the coordinated metals are expected to be potential descriptors for the rational design of efficient nitride catalysts.

2.4. Rational Design and Reaction Performance of Model Catalysts

To validate the reliability of the descriptors and realize the rational design, a series of model catalysts (including Co_3Mo_3N, Fe_3Mo_3N, Ni_3Mo_3N, and γ-Mo_2N) are synthesized. A set of X-ray diffraction (XRD) patterns are collected and correspond well to the standard powder patterns (Figure S24). High-resolution transmission electron microscopy (HR-TEM) images and energy-dispersive spectroscopy (EDS) elemental mapping further reveal the characteristic structures of metal nitrides and the homogeneous distribution of target elements (Figures S25−S29). All of these structural characterization results clearly demonstrate the successful synthesis of the target catalysts. The electronic states of the catalysts are monitored by *quasi in situ* XPS, and the magnetic metals in bimetallic nitrides exhibit metallic states (Figure S30), in agreement with theoretical calculations and previous reports.[46] These target catalysts are further evaluated in the CLAS reaction, where switching between Ar/H_2 (reaction gas) and N_2/H_2 (regeneration gas) is achieved via a four-way valve. Surprisingly, the mass reaction rate ($mmol_{NH3}/g_{cat}\cdot h$) of Mo_2N shows opposite results to the theoretical predictions (Figure S31), which might be attributed to the dramatic specific surface area difference between Mo_2N and bimetallic nitrides (Table S6).[67,68] Therefore, the reaction rate is normalized to the number of active sites ($mmol_{NH_3}/mmol_{site}\cdot h$), and the reaction performances of bimetallic nitrides exhibit marked improvements compared with Mo_2N (Figure 5a). Anomalous reaction performance trends illustrate that the Ni_3Mo_3N catalyst exhibits the highest intrinsic reactivity, which is nearly 1 order of magnitude higher compared to Mo_2N, while Mo_2N possesses more active sites for surface reaction. To better reveal the intrinsic activity of metal nitrides, a series of activation experiments are performed (Figure 5c,d). As shown in Figure 5b, the Ni_3Mo_3N catalyst shows a lower activation energy (35.0 kJ/mol) and lower H_2-TPR onset temperature (∼231 °C), indicating that a higher intrinsic activity is consistent with the results of CLAS reaction performance. The NH_3 signal integral area of H_2-TPR shows a significant relationship with the mass reaction rate, implying the high site density of Mo_2N (Figure S35). Furthermore, to assess the stability of the metal nitrides, a 30 cycle stability test was conducted (Figures 5e and S32). A stable NH_3 output without significant deactivation demonstrates that the metal nitrides can achieve stable lattice N-

https://doi.org/10.1021/jacsau.4c00194
JACS Au 2024, 4, 1975−1985

mediated ammonia production. However, these results bring a contradiction that Co_3Mo_3N was previously reported to be the most efficient catalyst in the literature.[53] On the one hand, this might be attributed to the difference of reaction mechanism between the conventional ammonia synthesis process and CLAS process for metal nitrides. More importantly, the crystal phase plays a key role in regulating the catalyst activity. Co_3Mo_3N and Fe_3Mo_3N phases are obtained for Co and Fe, while the Ni_2Mo_3N phase is gained for Ni with significantly different structures. By adjusting the annealing temperature, the Ni_3Mo_3N catalyst with higher activity can be obtained, which is predicted based on our proposed catalyst design principle. The Ni_2Mo_3N sample is also synthesized, and the structure and reaction performance are as expected compared with Ni_3Mo_3N (Figures S36−S38).

3. CONCLUSIONS

Rational design of transition metal nitride catalysts for lattice nitrogen-mediated ammonia synthesis processes is paramount to efficient and energy-saving ammonia production. Here, taking molybdenum-based metal nitrides as model catalysts, the multistage essences from microkinetic to microscopic structure are investigated to extract key intermediate species, rate-determining steps, and electronic structure characterizations. Using DFT computational energetics as bridges, the connection between catalyst intrinsic activity and electronic structure fingerprints is established. Based on the descriptors of charge transfer and spin magnetization, Ni_3Mo_3N is predicted to possess more excellent CLAS activity. A series of activation experiments confirm that the lattice nitrogen of Ni_3Mo_3N exhibits higher intrinsic activity and more efficient hydrogen response. Nevertheless, the overall rate and the specific descriptors exhibit a linear rather than volcanic relationship, which seems to violate Sabatier principle. The rate-determined step is not modified, and the interaction between active species and substrate does not overstep the volcanic peak due to the structural similarity among the model nitrides (Figure S39). This calls for us to expand the phase space of metal nitrides and include sample features to identify more universal descriptors. In addition, the contradiction between mass and active site reaction rate reveals the shortcomings of bimetallic nitrides, which require better dispersion for large-scale industrial applications. Overall, this work sheds light on realizing the paradigm shift from trial-and-error approach to rational design on a broader scale and provides strategies for the regulation and manipulation of the catalytic microenvironment.

4. METHODOLOGY

4.1. Chemicals and Materials

Ammonium molybdate tetrahydrate ($(NH_4)_6Mo_7O_{24}\cdot 4H_2O$, 99.0%) was purchased from Sinopharm. Nickel(II) nitrate hexahydrate ($Ni(NO_3)_2\cdot 6H_2O$, 99.99%) was purchased from Xilong Scientific. Cobaltous(II) nitrate hexahydrate ($Co(NO_3)_2\cdot 6H_2O$, 99.99%) and iron(III) nitrate nonahydrate ($Fe(NO_3)_3\cdot 9H_2O$, 99.99%) were purchased from Aladdin. N_2 (99.99%), H_2 (99.99%), and Ar (99.99%) were purchased from Beijing Huanyu Jinghui Gas. NH_3 (99.99%) were purchased from Air Liquide. The water used was deionized water (18.2 MΩ). All chemicals were used as received without further purification.

4.2. Preparation of Catalysts

4.2.1. Synthesis of M_3Mo_3N Catalysts (M = Co and Fe). The M_3Mo_3N catalysts were synthesized by the temperature-programmed nitridation of the oxide precursors. Taking Co as an example, 2 mmol of $(NH_4)_6Mo_7O_{24}\cdot 4H_2O$ and 14 mmol of $Co(NO_3)_2\cdot 6H_2O$ were dissolved in 180 mL of deionized water and mixed with magnetic stirring. Then, the mixture was added into a stainless steel reactor and hydrothermally synthesized at 160 °C for 6 h. The sample was washed with deionized water three times and then dried at 80 °C for 8 h. The desired $CoMoO_4$ precursor was obtained after calcination at 450 °C for 4 h in air. The $CoMoO_4$ precursor was ammonized at 850 °C for 3 h under a N_2/H_2 gas mixture (15 mL min^{-1} N_2 and 45 mL min^{-1} H_2) with a ramping rate of 10 °C min^{-1}. Subsequently, the gas was switched to N_2 gas for cooling. After cooling down to room temperature, the end of the tube furnace was opened, and the sample was passivated in air for 12 h.

4.2.2. Synthesis of Ni_nMo_3N Catalysts (n = 2 and 3). The Ni_nMo_3N catalysts were synthesized by the temperature-programmed nitridation of oxide precursors. 2 mmol of $(NH_4)_6Mo_7O_{24}\cdot 4H_2O$ and 14 mmol of $Ni(NO_3)_2\cdot 6H_2O$ were dissolved in 180 mL of deionized water and mixed with magnetic stirring. Then, the mixture was added into a stainless steel reactor and hydrothermally synthesized at 160 °C for 6 h. The sample was washed with deionized water three times and then dried at 80 °C for 8 h. The desired $NiMoO_4$ precursor was obtained after calcination at 450 °C for 4 h in air. For the nitridation process, different catalysts were obtained through changing the nitridation temperature. The Ni_3Mo_3N catalyst can be obtained at 700 °C for 1 h under a N_2/H_2 gas mixture (15 mL min^{-1} N_2 and 45 mL min^{-1} H_2) with a ramping rate of 10 °C·min^{-1}. The Ni_2Mo_3N catalyst can be obtained at 850 °C for 3 h under a N_2/H_2 gas mixture (15 mL min^{-1} N_2 and 45 mL min^{-1} H_2) with a ramping rate of 10 °C min^{-1}. Subsequently, the gas was switched to N_2 gas for cooling. After cooling down to room temperature, the end of the tube furnace was opened, and the sample was passivated in air for 12 h.

4.2.3. Synthesis of the γ-Mo_2N Catalyst. MoO_3 was obtained by calcination of $(NH_4)_6Mo_7O_{24}\cdot 4H_2O$ at 500 °C for 4 h. Then, the desired MoO_3 precursor was grounded and ammonized at 700 °C for 2 h under a NH_3 gas mixture (80 mL min^{-1} NH_3) with a two-stage temperature program, a ramping rate of 1 °C min^{-1} to 350 °C, and then a ramping rate of 5 °C min^{-1} to 700 °C. Subsequently, the gas was switched to N_2 gas for cooling and purging NH_3 gas. After cooling down to room temperature, the end of the tube furnace was opened, and the sample was passivated in air for 12 h. In this work, this sample was abbreviated as Mo_2N.

4.3. Catalytic Evaluations for Ammonia Production

The catalytic evaluations were carried out in a continuous-flow fixed-bed reactor under atmospheric pressure. A chemical looping process was performed to measure lattice nitrogen-mediated ammonia production. A pneumatic four-way valve was equipped to achieve the switching between H_2/N_2 (25/75%) and H_2/Ar (25/75%). Typically, 100 mg catalyst (40−60 mesh) was loaded into a quartz tube with an inner diameter of 4 mm and fixed by quartz wool. Then, the catalysts were pretreated at 600 °C for 1 h under a N_2/H_2 gas mixture (10 mL min^{-1} N_2 and 30 mL min^{-1} H_2) with a ramping rate of 10 °C min^{-1}. Then, the reactor was cooled to reaction temperature to perform the reactivity tests. The total flow was kept at 40 mL·min^{-1} to minimize the effects of pressure fluctuations during switching.

https://doi.org/10.1021/jacsau.4c00194
JACS Au 2024, 4, 1975−1985

The output gas was introduced into a diluted H_2SO_4 solution (1 mmol/L, 200 mL at 30 °C), and the ion conductivity was monitored by a conductivity meter (Mettler Toledo SevenMulti) to quantify ammonia production.

4.4. Characterizations

4.4.1. Powder XRD. Phase analysis was identified by XRD (D8 Advance equipped with Cu Kα radiation). The diffraction data was collected between 5 and 90° at a rate of 5°·min^{-1}.

4.4.2. High-Resolution Transmission Electron Microscopy. Images of the catalyst morphology were obtained by HR-TEM (JSM2010, at 200 keV).

4.4.3. Inductively Coupled Plasma-Optical Emission Spectroscopy. Elemental compositions were measured by inductively coupled plasma-optical emission spectroscopy (iCAP Q). The catalysts (20 mg) were solubilized with aqua regia (5 mL) and HF (5 mL) at 180 °C. The solution was vaporized and then resolubilized in an aqueous solution (100 mL).

4.4.4. N_2 Physical Adsorption. The specific surface area (S_{BET}) was determined by N_2 adsorption isotherms (Quantachrome Autosorb-6B analyzer). The N_2 adsorption was carried out at 77 K in the pressure range of p/p_0 = 0.05−0.30, and the specific surface area was calculated using the Brunauer−Emmett−Teller (BET) method.

4.4.5. Quasi-In Situ XPS. The surface elemental distributions were analyzed by quasi-in situ XPS (AXIS SUPRA+). The samples were pretreated in the reaction chamber at 600 °C for 2 h under a N_2/H_2 gas mixture (5 mL min^{-1} N_2 and 15 mL min^{-1} H_2) and then moved to the sample chamber without air exposure.

4.5. Computational Details

The DFT calculations were carried out with the dispersion corrections by the D3 method of Grimme (DFT-D3) using VASP 5.4.4.[69,70] The projector augmented wave method was used to describe the interaction of the atomic cores and valence electrons.[71,72] The Perdew−Burke−Ernzerhof generalized gradient approximation was used to calculate the exchange−correlation energy.[73] The kinetics energy cutoff was set as 450 eV with a Gaussian smearing of 0.1 eV. The convergence threshold for electronic steps and ionic steps were set as 10^{-5} eV and 0.03 eV Å^{-1}, respectively. The initial structure models for M_3Mo_3N were obtained from Materials Project database:[74] Co_3Mo_3N (mp-22166), Fe_3Mo_3N (mp-510619), and Ni_3Mo_3N (mp-581805). For all samples, four-layer p (2 × 2) supercells of the (111) facet were built to investigate the catalytic reaction. It is worth mentioning that a stoichiometric Mo_2N (111) model would expose Mo on one side (denoted as Mo terminal) and N on the other (denoted as N terminal), which was accompanied by polar, so we moved half of N atoms to the Mo-terminated surface.[75] The top two atomic layers were relaxed, and a vacuum region of 15 Å was created. The Monkhorst−Pack scheme was used to generate a k-point grid in the Brillouin zone. (1 × 1 × 1) and (3 × 3 × 1) k-point grid was adopted for M_3Mo_3N and Mo_2N, respectively. The TS was determined by climbing image nudged elastic band method and dimer method.[76,77] Vibrational analysis was performed to confirm the TSs with only one imaginary frequency. For all electron energies, zero-point energy corrections were also considered.

4.6. Microkinetic Model

The mean-field MKM was used to measure reaction rate information. The TOF and the coverage of the reaction intermediates can be obtained by solving a set of ordinary differential equations

$$\frac{\partial \theta_i}{\partial t} = 0 \tag{1}$$

$$\sum_i \theta_i = 1 \tag{2}$$

where θ_i is the coverage of the surface species i. $\frac{\partial \theta_i}{\partial t} = 0$ can be determined by the rate expressions for elementary reactions

$$r_i = k_i^{\mathrm{f}} \prod_j \theta_{ij} \prod_j p_{ij} - k_i^{\mathrm{r}} \prod_k \theta_{ik} \prod_k p_{ik} \tag{3}$$

where r_i is the rate of reaction intermediates i, $p_{ij}(p_{ik})$ is the partial pressure of gas-phase reactants (or products), and k_i^{f} and k_i^{r} are the forward and reverse rate constants, respectively. The analysis of DRC was carried out to obtain the information about RDS.[54−56]

■ ASSOCIATED CONTENT

Supporting Information

The Supporting Information is available free of charge at https://pubs.acs.org/doi/10.1021/jacsau.4c00194.

Details of experimental and computational methods; reaction networks of lattice nitrogen-mediated ammonia production; structure characterization of the catalyst; reaction performance for chemical looping; structures for surface adsorption species; and electronic structure (PDF)

(ZIP)

■ AUTHOR INFORMATION

Corresponding Author

Yi Cheng − *Department of Chemical Engineering, Tsinghua University, Beijing 100084, P. R. China;* orcid.org/0000-0002-0711-1884; Email: yicheng@tsinghua.edu.cn

Authors

Shuairen Qian − *Department of Chemical Engineering, Tsinghua University, Beijing 100084, P. R. China*

Tianying Dai − *Department of Chemical Engineering, Tsinghua University, Beijing 100084, P. R. China*

Kai Feng − *Institute of Functional Nano & Soft Materials (FUNSOM), Soochow University, Suzhou, Jiangsu 215123, P. R. China*

Zhengwen Li − *Department of Chemical Engineering, Tsinghua University, Beijing 100084, P. R. China*

Xiaohang Sun − *Department of Chemical Engineering, Tsinghua University, Beijing 100084, P. R. China*

Yuxin Chen − *Department of Chemical Engineering, Tsinghua University, Beijing 100084, P. R. China;* orcid.org/0000-0002-4622-8516

Kaiqi Nie − *Department of Chemical Engineering, Tsinghua University, Beijing 100084, P. R. China*

Binhang Yan − *Department of Chemical Engineering, Tsinghua University, Beijing 100084, P. R. China;* orcid.org/0000-0003-2833-8022

Complete contact information is available at: https://pubs.acs.org/10.1021/jacsau.4c00194

Notes

The authors declare no competing financial interest.

■ ACKNOWLEDGMENTS

This work was financially supported by the National Natural Science Foundation of China (nos. 22278235, 21991104, and 22250710677). This work was also supported by the Tsinghua National Laboratory for Information Science and Technology.

■ REFERENCES

(1) Chen, J. G.; Crooks, R. M.; Seefeldt, L. C.; Bren, K. L.; Bullock, R. M.; Darensbourg, M. Y.; Holland, P. L.; Hoffman, B.; Janik, M. J.; Jones, A. K.; Kanatzidis, M. G.; King, P.; Lancaster, K. M.; Lymar, S. V.; Pfromm, P.; Schneider, W. F.; Schrock, R. R. Beyond Fossil Fuel-Driven Nitrogen Transformations. *Science* **2018**, *360* (6391), No. eaar6611.
(2) Erisman, J. W.; Sutton, M. A.; Galloway, J.; Klimont, Z.; Winiwarter, W. How a Century of Ammonia Synthesis Changed the World. *Nat. Geosci.* **2008**, *1*, 636−639.
(3) Guo, J.; Chen, P. Catalyst: NH_3 as an Energy Carrier. *Chem* **2017**, *3* (5), 709−712.
(4) Schlögl, R. Catalytic Synthesis of Ammonia−A "Never-Ending Story"? *Angew. Chem., Int. Ed.* **2003**, *42* (18), 2004−2008.
(5) Liu, H. Ammonia Synthesis Catalyst 100 Years: Practice, Enlightenment and Challenge. *Chin. J. Catal.* **2014**, *35* (10), 1619−1640.
(6) Wang, M.; Khan, M. A.; Mohsin, I.; Wicks, J.; Ip, A. H.; Sumon, K. Z.; Dinh, C.-T.; Sargent, E. H.; Gates, I. D.; Kibria, M. G. Can Sustainable Ammonia Synthesis Pathways Compete with Fossil-Fuel Based Haber-Bosch Processes? *Energy Environ. Sci.* **2021**, *14* (5), 2535−2548.
(7) Michalsky, R.; Avram, A. M.; Peterson, B. A.; Pfromm, P. H.; Peterson, A. A. Chemical Looping of Metal Nitride Catalysts: Low-Pressure Ammonia Synthesis for Energy Storage. *Chem. Sci.* **2015**, *6* (7), 3965−3974.
(8) Gao, W.; Guo, J.; Wang, P.; Wang, Q.; Chang, F.; Pei, Q.; Zhang, W.; Liu, L.; Chen, P. Production of Ammonia via a Chemical Looping Process Based on Metal Imides as Nitrogen Carriers. *Nat. Energy* **2018**, *3* (12), 1067−1075.
(9) Nguyen, N. P.; Kaur, S.; Bush, H. E.; Miller, J. E.; Ambrosini, A.; Loutzenhiser, P. G. Two-Step Chemical Looping Cycle for Renewable NH_3 Production Based on Non-Catalytic Co_3Mo_3N/Co_6Mo_6N Reactions. *Adv. Energy Mater.* **2023**, *14*, 2302740.
(10) Wang, B.; Shen, L. Recent Advances in NH_3 Synthesis with Chemical Looping Technology. *Ind. Eng. Chem. Res.* **2022**, *61* (50), 18215−18231.
(11) Brown, S.; Hu, J. Review of Chemical Looping Ammonia Synthesis Materials. *Chem. Eng. Sci.* **2023**, *280*, 119063.
(12) Feng, S.; Gao, W.; Wang, Q.; Guan, Y.; Yan, H.; Wu, H.; Cao, H.; Guo, J.; Chen, P. A Multi-Functional Composite Nitrogen Carrier for Ammonia Production via a Chemical Looping Route. *J. Mater. Chem. A* **2021**, *9* (2), 1039−1047.
(13) Goto, Y.; Daisley, A.; Hargreaves, J. S. J. Towards Anti-Perovskite Nitrides as Potential Nitrogen Storage Materials for Chemical Looping Ammonia Production: Reduction of Co_3ZnN, Ni_3ZnN, Co_3InN and Ni_3InN under Hydrogen. *Catal. Today* **2021**, *364*, 196−201.
(14) Sun, Z.; Li, K.; Toan, S.; Zhang, R.; Li, H.; Wu, Y.; Sun, Z. Ammonia Synthesis via Chromium-Based Nitrogen Carrier Looping. *Chem. Eng. J.* **2023**, *476*, 146643.
(15) Wang, S.; Gong, F.; Zhou, Q.; Xie, Y.; Li, H.; Li, M.; Fu, E.; Yang, P.; Jing, Y.; Xiao, R. Transition Metal Enhanced Chromium Nitride as Composite Nitrogen Carrier for Sustainable Chemical Looping Ammonia Synthesis. *Appl. Catal. B Environ.* **2023**, *339*, 123134.
(16) Ye, T.-N.; Park, S.-W.; Lu, Y.; Li, J.; Sasase, M.; Kitano, M.; Hosono, H. Contribution of Nitrogen Vacancies to Ammonia Synthesis over Metal Nitride Catalysts. *J. Am. Chem. Soc.* **2020**, *142* (33), 14374−14383.
(17) Ye, T.-N.; Park, S.-W.; Lu, Y.; Li, J.; Sasase, M.; Kitano, M.; Tada, T.; Hosono, H. Vacancy-Enabled N_2 Activation for Ammonia Synthesis on an Ni-Loaded Catalyst. *Nature* **2020**, *583* (7816), 391−395.
(18) Ye, T.-N.; Park, S.-W.; Lu, Y.; Li, J.; Wu, J.; Sasase, M.; Kitano, M.; Hosono, H. Dissociative and Associative Concerted Mechanism for Ammonia Synthesis over Co-Based Catalyst. *J. Am. Chem. Soc.* **2021**, *143* (32), 12857−12866.
(19) Lu, Y.; Ye, T.; Li, J.; Li, Z.; Guan, H.; Sasase, M.; Niwa, Y.; Abe, H.; Li, Q.; Pan, F.; Kitano, M.; Hosono, H. Approach to Chemically Durable Nickel and Cobalt Lanthanum-Nitride-Based Catalysts for Ammonia Synthesis. *Angew. Chem., Int. Ed.* **2022**, *134* (47), No. e202211759.
(20) Li, Z.; Lu, Y.; Li, J.; Xu, M.; Qi, Y.; Park, S.-W.; Kitano, M.; Hosono, H.; Chen, J.-S.; Ye, T.-N. Multiple Reaction Pathway on Alkaline Earth Imide Supported Catalysts for Efficient Ammonia Synthesis. *Nat. Commun.* **2023**, *14* (1), 6373.
(21) Garden, A. L.; Abghoui, Y.; Skúlason, E. Applications of transition metal nitrides as electrocatalysts. In *Alternative Catalytic Materials: Carbides, Nitrides, Phosphides and Amorphous Boron Alloys*; Royal Society of Chemistry, 2018.
(22) Abghoui, Y.; Garden, A. L.; Hlynsson, V. F.; Björgvinsdóttir, S.; Ólafsdóttir, H.; Skúlason, E. Enabling Electrochemical Reduction of Nitrogen to Ammonia at Ambient Conditions through Rational Catalyst Design. *Phys. Chem. Chem. Phys.* **2015**, *17* (7), 4909−4918.
(23) Abghoui, Y.; Garden, A. L.; Howalt, J. G.; Vegge, T.; Skúlason, E. Electroreduction of N_2 to Ammonia at Ambient Conditions on Mononitrides of Zr, Nb, Cr, and V: A DFT Guide for Experiments. *ACS Catal.* **2016**, *6* (2), 635−646.
(24) Abghoui, Y.; Skúlason, E. Computational Predictions of Catalytic Activity of Zincblende (110) Surfaces of Metal Nitrides for Electrochemical Ammonia Synthesis. *J. Phys. Chem. C* **2017**, *121* (11), 6141−6151.
(25) Abghoui, Y.; Skúlason, E. Electrochemical Synthesis of Ammonia via Mars-van Krevelen Mechanism on the (111) Facets of Group III-VII Transition Metal Mononitrides. *Catal. Today* **2017**, *286*, 78−84.
(26) Abghoui, Y.; Skúlason, E. Onset Potentials for Different Reaction Mechanisms of Nitrogen Activation to Ammonia on Transition Metal Nitride Electro-Catalysts. *Catal. Today* **2017**, *286*, 69−77.
(27) Abghoui, Y.; Iqbal, A.; Skúlason, E. The Role of Overlayered Nitride Electro-Materials for N_2 Reduction to Ammonia. *Front. Catal.* **2023**, *2*, 1096824.
(28) Sun, W.; Holder, A.; Orvañanos, B.; Arca, E.; Zakutayev, A.; Lany, S.; Ceder, G. Thermodynamic Routes to Novel Metastable Nitrogen-Rich Nitrides. *Chem. Mater.* **2017**, *29* (16), 6936−6946.
(29) Sun, W.; Bartel, C. J.; Arca, E.; Bauers, S. R.; Matthews, B.; Orvañanos, B.; Chen, B.-R.; Toney, M. F.; Schelhas, L. T.; Tumas, W.; Tate, J.; Zakutayev, A.; Lany, S.; Holder, A. M.; Ceder, G. A Map of the Inorganic Ternary Metal Nitrides. *Nat. Mater.* **2019**, *18* (7), 732−739.
(30) Tian, D.; Denny, S. R.; Li, K.; Wang, H.; Kattel, S.; Chen, J. G. Density Functional Theory Studies of Transition Metal Carbides and Nitrides as Electrocatalysts. *Chem. Soc. Rev.* **2021**, *50* (22), 12338−12376.
(31) Wang, H.; Li, J.; Li, K.; Lin, Y.; Chen, J.; Gao, L.; Nicolosi, V.; Xiao, X.; Lee, J.-M. Transition Metal Nitrides for Electrochemical Energy Applications. *Chem. Soc. Rev.* **2021**, *50* (2), 1354−1390.
(32) Feng, Q.; Zhao, S.; Wang, Y.; Dong, J.; Chen, W.; He, D.; Wang, D.; Yang, J.; Zhu, Y.; Zhu, H.; Gu, L.; Li, Z.; Liu, Y.; Yu, R.; Li, J.; Li, Y. Isolated Single-Atom Pd Sites in Intermetallic Nanostructures: High Catalytic Selectivity for Semihydrogenation of Alkynes. *J. Am. Chem. Soc.* **2017**, *139* (21), 7294−7301.
(33) Jiang, C.; Song, H.; Sun, G.; Chang, X.; Zhen, S.; Wu, S.; Zhao, Z.-J.; Gong, J. Data-Driven Interpretable Descriptors for the Structure−Activity Relationship of Surface Lattice Oxygen on Doped Vanadium Oxides. *Angew. Chem., Int. Ed.* **2022**, *61* (35), No. e202206758.
(34) Chang, X.; Zhao, Z.-J.; Lu, Z.; Chen, S.; Luo, R.; Zha, S.; Li, L.; Sun, G.; Pei, C.; Gong, J. Designing Single-Site Alloy Catalysts Using a Degree-of-Isolation Descriptor. *Nat. Nanotechnol.* **2023**, *18*, 611−616.
(35) Han, Z.; Gao, R.; Wang, T.; Tao, S.; Jia, Y.; Lao, Z.; Zhang, M.; Zhou, J.; Li, C.; Piao, Z.; Zhang, X.; Zhou, G. Machine-Learning-

https://doi.org/10.1021/jacsau.4c00194
JACS Au 2024, 4, 1975−1985

Assisted Design of a Binary Descriptor to Decipher Electronic and Structural Effects on Sulfur Reduction Kinetics. *Nat. Catal.* **2023**, *6*, 1073−1086.
(36) Ren, C.; Li, Q.; Ling, C.; Wang, J. Mechanism-Guided Design of Photocatalysts for CO_2 Reduction toward Multicarbon Products. *J. Am. Chem. Soc.* **2023**, *145* (51), 28276−28283.
(37) Chen, W.; Cao, J.; Yang, J.; Cao, Y.; Zhang, H.; Jiang, Z.; Zhang, J.; Qian, G.; Zhou, X.; Chen, D.; Yuan, W.; Duan, X. Molecular-Level Insights into the Electronic Effects in Platinum-Catalyzed Carbon Monoxide Oxidation. *Nat. Commun.* **2021**, *12* (1), 6888.
(38) Bruix, A.; Margraf, J. T.; Andersen, M.; Reuter, K. First-Principles-Based Multiscale Modelling of Heterogeneous Catalysis. *Nat. Catal.* **2019**, *2* (8), 659−670.
(39) Chen, W.; Qian, G.; Wan, Y.; Chen, D.; Zhou, X.; Yuan, W.; Duan, X. Mesokinetics as a Tool Bridging the Microscopic-to-Macroscopic Transition to Rationalize Catalyst Design. *Acc. Chem. Res.* **2022**, *55* (22), 3230−3241.
(40) Mitchell, S.; Martín, A. J.; Pérez-Ramírez, J. Transcending Scales in Catalysis for Sustainable Development. *Nat. Chem. Eng.* **2024**, *1* (1), 13−15.
(41) Howalt, J. G.; Vegge, T. Electrochemical Ammonia Production on Molybdenum Nitride Nanoclusters. *Phys. Chem. Chem. Phys.* **2013**, *15* (48), 20957.
(42) Zeinalipour-Yazdi, C. D.; Hargreaves, J. S. J.; Catlow, C. R. A. Nitrogen Activation in a Mars-van Krevelen Mechanism for Ammonia Synthesis on Co_3Mo_3N. *J. Phys. Chem. C* **2015**, *119* (51), 28368−28376.
(43) Zeinalipour-Yazdi, C. D.; Hargreaves, J. S. J.; Catlow, C. R. A. DFT-D3 Study of Molecular N_2 and H_2 Activation on Co_3Mo_3N Surfaces. *J. Phys. Chem. C* **2016**, *120* (38), 21390−21398.
(44) Zeinalipour-Yazdi, C. D.; Hargreaves, J. S. J.; Catlow, C. R. A. Low-T Mechanisms of Ammonia Synthesis on Co_3Mo_3N. *J. Phys. Chem. C* **2018**, *122* (11), 6078−6082.
(45) Qian, S.; Feng, K.; Li, Z.; Chen, Y.; Sun, X.; Wang, Y.; Yan, B.; Cheng, Y. Insight into the Dynamic Evolution of Co_3Mo_3N Bimetallic Nitride Surface during Ammonia Synthesis. *ACS Catal.* **2023**, *13* (21), 13931−13940.
(46) Feng, K.; Tian, J.; Zhang, J.; Li, Z.; Chen, Y.; Luo, K. H.; Yang, B.; Yan, B. Dual Functionalized Interstitial N Atoms in Co_3Mo_3N Enabling CO_2 Activation. *ACS Catal.* **2022**, *12* (8), 4696−4706.
(47) Ravi, M.; Makepeace, J. W. Facilitating Green Ammonia Manufacture under Milder Conditions: What Do Heterogeneous Catalyst Formulations Have to Offer? *Chem. Sci.* **2022**, *13* (4), 890−908.
(48) Jacobsen, C. J. H.; Dahl, S.; Clausen, B. S.; Bahn, S.; Logadottir, A.; Nørskov, J. K. Catalyst Design by Interpolation in the Periodic Table: Bimetallic Ammonia Synthesis Catalysts. *J. Am. Chem. Soc.* **2001**, *123* (34), 8404−8405.
(49) Logadottir, A.; Rod, T. H.; Nørskov, J.; Hammer, B.; Dahl, S.; Jacobsen, C. J. H. The Brønsted−Evans−Polanyi Relation and the Volcano Plot for Ammonia Synthesis over Transition Metal Catalysts. *J. Catal.* **2001**, *197* (2), 229−231.
(50) Kozuch, S.; Shaik, S. How to Conceptualize Catalytic Cycles? The Energetic Span Model. *Acc. Chem. Res.* **2011**, *44* (2), 101−110.
(51) Bac, S.; Mallikarjun Sharada, S. CO Oxidation with Atomically Dispersed Catalysts: Insights from the Energetic Span Model. *ACS Catal.* **2022**, *12* (3), 2064−2076.
(52) Alconchel, S.; Sapiña, F.; Beltrán, D.; Beltrán, A. Chemistry of Interstitial Molybdenum Ternary Nitrides M_nMo_3N (M = Fe, Co, N = 3; M = Ni, N = 2). *J. Mater. Chem.* **1998**, *8* (8), 1901−1909.
(53) Jacobsen, C. J. H. Novel Class of Ammonia Synthesis Catalysts. *Chem. Commun.* **2000**, *12* (12), 1057−1058.
(54) Campbell, C. T. Future Directions and Industrial Perspectives Micro- and Macro-Kinetics: Their Relationship in Heterogeneous Catalysis. *Top. Catal.* **1994**, *1* (3−4), 353−366.
(55) Campbell, C. T. Finding the Rate-Determining Step in a Mechanism. *J. Catal.* **2001**, *204* (2), 520−524.
(56) Campbell, C. T. The Degree of Rate Control: A Powerful Tool for Catalysis Research. *ACS Catal.* **2017**, *7* (4), 2770−2779.
(57) Peng, J.; Giner-Sanz, J. J.; Giordano, L.; Mounfield, W. P.; Leverick, G. M.; Yu, Y.; Román-Leshkov, Y.; Shao-Horn, Y. Design Principles for Transition Metal Nitride Stability and Ammonia Generation in Acid. *Joule* **2023**, *7* (1), 150−167.
(58) Camellone, M. F.; Fabris, S. Reaction Mechanisms for the CO Oxidation on Au/CeO_2 Catalysts: Activity of Substitutional Au^{3+}/Au^{+} Cations and Deactivation of Supported Au^{+} Adatoms. *J. Am. Chem. Soc.* **2009**, *131* (30), 10473−10483.
(59) Seo, D.-H.; Lee, J.; Urban, A.; Malik, R.; Kang, S.; Ceder, G. The Structural and Chemical Origin of the Oxygen Redox Activity in Layered and Cation-Disordered Li-Excess Cathode Materials. *Nat. Chem.* **2016**, *8* (7), 692−697.
(60) Fung, V.; Wu, Z.; Jiang, D. New Bonding Model of Radical Adsorbate on Lattice Oxygen of Perovskites. *J. Phys. Chem. Lett.* **2018**, *9* (21), 6321−6325.
(61) Cao, A.; Bukas, V. J.; Shadravan, V.; Wang, Z.; Li, H.; Kibsgaard, J.; Chorkendorff, I.; Nørskov, J. K. A Spin Promotion Effect in Catalytic Ammonia Synthesis. *Nat. Commun.* **2022**, *13* (1), 2382.
(62) Xu, G.; Cai, C.; Wang, T. Toward Sabatier Optimal for Ammonia Synthesis with Paramagnetic Phase of Ferromagnetic Transition Metal Catalysts. *J. Am. Chem. Soc.* **2022**, *144* (50), 23089−23095.
(63) Zhang, D.; Li, H.; Lu, H.; Yin, Z.; Fusco, Z.; Riaz, A.; Reuter, K.; Catchpole, K.; Karuturi, S. Unlocking the Performance of Ternary Metal (Hydro)Oxide Amorphous Catalysts via Data-Driven Active-Site Engineering. *Energy Environ. Sci.* **2023**, *16* (11), 5065−5075.
(64) Hammer, B.; Norskov, J. K. Why Gold Is the Noblest of All the Metals. *Nature* **1995**, *376* (6537), 238−240.
(65) Nørskov, J. K.; Abild-Pedersen, F.; Studt, F.; Bligaard, T. Density Functional Theory in Surface Chemistry and Catalysis. *Proc. Natl. Acad. Sci. U.S.A.* **2011**, *108* (3), 937−943.
(66) Miedema, A. R. The Electronegativity Parameter for Transition Metals: Heat of Formation and Charge Transfer in Alloys. *J. Less Common. Met.* **1973**, *32* (1), 117−136.
(67) Hargreaves, J. S. J.; Mckay, D. A Comparison of the Reactivity of Lattice Nitrogen in Co_3Mo_3N and Ni_2Mo_3N Catalysts. *J. Mol. Catal. Chem.* **2009**, *305* (1−2), 125−129.
(68) Podila, S.; Zaman, S. F.; Driss, H.; Al-Zahrani, A. A.; Daous, M. A.; Petrov, L. A. High Performance of Bulk Mo_2N and Co_3Mo_3N Catalysts for Hydrogen Production from Ammonia: Role of Citric Acid to Mo Molar Ratio in Preparation of High Surface Area Nitride Catalysts. *Int. J. Hydrogen Energy* **2017**, *42* (12), 8006−8020.
(69) Kresse, G.; Furthmüller, J. Efficiency of Ab-Initio Total Energy Calculations for Metals and Semiconductors Using a Plane-Wave Basis Set. *Comput. Mater. Sci.* **1996**, *6* (1), 15−50.
(70) Grimme, S.; Ehrlich, S.; Goerigk, L. Effect of the Damping Function in Dispersion Corrected Density Functional Theory. *J. Comput. Chem.* **2011**, *32* (7), 1456−1465.
(71) Kresse, G.; Furthmüller, J. Efficient Iterative Schemes for Ab Initio Total-Energy Calculations Using a Plane-Wave Basis Set. *Phys. Rev. B* **1996**, *54* (16), 11169−11186.
(72) Kresse, G.; Joubert, D. From Ultrasoft Pseudopotentials to the Projector Augmented-Wave Method. *Phys. Rev. B* **1999**, *59* (3), 1758−1775.
(73) Perdew, J. P.; Burke, K.; Ernzerhof, M. Generalized Gradient Approximation Made Simple. *Phys. Rev. Lett.* **1996**, *77* (18), 3865−3868.
(74) Jain, A.; Ong, S. P.; Hautier, G.; Chen, W.; Richards, W. D.; Dacek, S.; Cholia, S.; Gunter, D.; Skinner, D.; Ceder, G.; Persson, K. A. Commentary: The Materials Project: A Materials Genome Approach to Accelerating Materials Innovation. *APL Mater.* **2013**, *1* (1), 011002.
(75) Zhao, J.; Cui, C.; Wang, H.; Han, J.; Zhu, X.; Ge, Q. Insights into the Mechanism of Ammonia Decomposition on Molybdenum Nitrides Based on DFT Studies. *J. Phys. Chem. C* **2019**, *123* (1), 554−564.
(76) Henkelman, G.; Uberuaga, B. P.; Jónsson, H. A Climbing Image Nudged Elastic Band Method for Finding Saddle Points and Minimum Energy Paths. *J. Chem. Phys.* **2000**, *113* (22), 9901−9904.
(77) Henkelman, G.; Jónsson, H. A Dimer Method for Finding Saddle Points on High Dimensional Potential Surfaces Using Only First Derivatives. *J. Chem. Phys.* **1999**, *111* (15), 7010−7022.

https://doi.org/10.1021/jacsau.4c00194
JACS Au 2024, 4, 1975−1985